INSTITUTO DE FÍSICA

preprint

IFUSP/P-237

LEADING NON-CANCELLING INFRA-RED DIVERGENCES IN PERTURBATIVE QCD

C. E. Carneiro, M. Day, J. Frenkel,
J. C. Taylor and M. T. Thomaz

UNIVERSIDADE DE SÃO PAULO
INSTITUTO DE FÍSICA
Caixa Postal - 20.516
Cidade Universitária
São Paulo - BRASIL

LEADING NON-CANCELLING INFRA-RED DIVERGENCES IN PERTURBATIVE QCD

C. E. Carneiro
Instituto de Física, USP, São Paulo, Brasil,

M. Day
DAMTP, University of Cambridge, Cambridge, England and
Dept. Theoretical Physics, Oxford University, Oxford, England,

J. Frenkel
Instituto de Física, USP, São Paulo, Brasil,

J. C. Taylor
DAMTP, University of Cambridge, Cambridge, England and
Dept. Theoretical Physics, Oxford University, Oxford, England,

M. T. Thomaz
Instituto de Física, USP, São Paulo, Brasil.

Abstract

In QCD in perturbative theory, for the inclusive cross-section for the scattering of two coloured particles, we identify graphs which contribute to the general leading order $\alpha_s (\alpha_s \ln \lambda)^n$ and we sum these contributions (λ is the IR cut-off). The work is done in the Coulomb gauge; an appendix discusses the Feynman gauge.

(1980)

1. Introduction

In previous papers [1, 2, 3, 4] it has been shown that the Bloch-Nordsieck mechanism for the cancellation of soft (IR) divergences in perturbation theory does not work in QCD when there are two coloured particles (colour-averaged) in the initial state. The uncancelled IR divergence which has been calculated is that of lowest order, $\alpha_s^2 / n\lambda$, where α_s is the coupling strength ($g^2/4\pi$) and λ is some IR cut-off. In the present paper, we try to identify and sum all leading order uncancelled IR divergences. These are of order $\alpha_s(\alpha_s/n\lambda)^n$. One reason for doing this, is to see whether the infinity becomes a zero when the series is summed (as it does, for example, with the virtual IR divergences in QED). We discuss this question in Section 4. Of course, we cannot give a conclusive answer, because we sum only the leading divergences.

In most of this paper we use the Coulomb gauge in the rest system of one of the initial particles, because we found in reference [3] that it shortened the work. We also find that the Coulomb gauge gives more physical insight than the Feynman gauge. However, we include an Appendix (A) showing how the Feynman gauge can be used to demonstrate directly the non-cancellation of IR divergences, as was done in the Coulomb gauge in Section 2 of reference [3]. This work has been briefly reported in reference [2].

In [3] we used the simple example

$$q + \bar{q} \longrightarrow \gamma^* + (\text{soft gluons}) \qquad (1)$$

because it is the simplest process with two coloured particles in the initial state. However, the arguments used in [1] and [4] strongly suggest that the non-cancelling divergences are a property of the initial state alone. Then, we can as easily study the more general reaction

$$q + Q \longrightarrow (\text{final state including soft gluons}) \qquad (2)$$

where q and Q are two coloured particles, with non-zero mass, which we call "quarks" for short. We can allow q and Q to belong to different representations of the colour group, with matrix generators t_a and T_a ($a = 1, \ldots \nu$, where ν is the order of the group). This also provides a useful check on the results, since the complete answer must be symmetric under the interchange $t \leftrightarrow T$, although the gauge we use (the Coulomb gauge in the rest frame of Q) destroys the symmetry in individual terms.

For purely technical reasons, we use dimensional IR regularization with space-time dimension $4 + \eta$. The IR cut-off mentioned is related to η by

$$\eta^{-1} = -\ln \lambda + (\text{finite terms}) \tag{3}$$

We express our results in terms of the laboratory frame speed β, related to the centre-of-mass energy squared, s, by

$$1 - \beta^2 = \left[\frac{s}{2m^2} - 1 \right]^{-2} \tag{4}$$

The Casimir invariant of the adjoint representation is C_G:

$$f_{abc} f_{abd} = C_G \delta_{cd} \tag{5}$$

where f_{abc} are the structure constants.

We shall also need a notation for the "hard" part of the Feynman graphs, which in the simplest case is just the Born approximation (for a definition of "hard" in this context, see [1] and [4]). Let the "hard" amplitude be M_H, and define

$$H = M_H^* M_H \tag{6}$$

Here a sum over final colours is understood, but not over initial ones, so that H is a matrix in the direct product of the representation spaces of q and Q. (Spins are irrelevant in the eikonal approximation, which we always assume to be valid. This approximation is discussed in [1], [3] and [4]).

With all this notation, we may state our result :

$$2\,\mathrm{Tr}\,(t.T\,H)\,C_G\,(\rho^{-1}-1)\,F(\beta)\int_0^{\Delta} du\,u^{-1}\left(\frac{u}{\mu}\right)^{2\eta}\alpha_s^2(u)\,\times$$

$$\times\ \exp\left[-\pi^{-1}\,C_G\,F(\beta)\int_{\mu}^{\Delta} dq\ q^{-1}\left(\frac{q}{\mu}\right)^{\eta}\alpha_s(q)\right] \qquad (7)$$

Here

$$F(\beta)\equiv(2\beta)^{-1}\ln\left(\frac{1+\beta}{1-\beta}\right)-1 \qquad (8)$$

is a function appearing in QED IR divergences, μ is an arbitrary unit of mass appearing in renormalization, and $\alpha_s(q)$ is the running coupling-strength. To be consistent with our leading-logarithm calculation, $\alpha_s(q)$ ought to be written in leading-logarithm approximation

$$[\alpha_s(q)]^{-1}=[\alpha_s(\mu)]^{-1}+\frac{11}{6\pi}\,C_G\,\eta^{-1}\left[\left(\frac{q}{\mu}\right)^{\eta}-1\right] \qquad (9)$$

In Section 4, we discuss the result (7) and find its limiting behaviour under a set of particular assumptions. We make some remarks about the physical significance of the non-cancelling IR divergences. Section 2 is about what we call "ladder" diagrams, which give (7) without the running coupling constant (i.e., with $\alpha_s(u)$ and $\alpha_s(q)$ each replaced by a constant value α_s in (7)). Section 3 is about renormalization graphs, which we argue, make the coupling constant run. Although this result is not rigorously proved, we give some general lines of the argument, and examine a few illustrative cases in detail.

The main guiding idea we use in identifying the leading divergences is the principle of what we will call "nested divergences". We explain this by a simple example. Suppose there is an integral over the lengths, k_1 and k_2, of two three-momenta. Let

$$u=k_1+k_2 \qquad\qquad v=\frac{k_1}{k_2} \qquad (10)$$

In order to get a leading, doubly logarithmic IR divergence the u - integral must diverge at $u=0$ and the v - integral must diverge at $v=0$ or ∞, let us say, $v=0$. In order to calculate the coefficient of the double-logarithm, we may put $v=0$ under

the u - integral. This is equivalent to neglecting k_1 compared with k_2 in those denominators which depend upon k_1 and k_2, provided that we restrict the ranges of integration by $k_1 < k_2$.

In order to obtain a leading divergence in this way, it is necessary that the subdiagram obtained by omitting all lines which depend only on k_1 should itself be IR divergent (when its external lines are on-shell). In such a case we shall describe this subdiagram as being nested inside the complete diagram. Similarly, the diagram made up of the lines which depend on k_1 only (the above subdiagram being reduced to a "blob") is also divergent by itself.

This principle is certainly well supported by experience with real and virtual IR divergences separately. In our case, where we are concerned with IR divergences that remain after some cancellation between real and virtual, we should, perhaps, use it with some caution. In Appendix B we describe an example in which we have tested it, and in which it is found to work.

In Figure (1a) we show a typical diagram that contributes to order $\alpha_s^2 \eta^{-1}$, as in references [1, 2, 3, 4]. One way of generating higher order leading diagrams is to nest subdivergences into the vertices of Figure (1a). If they are nested into the quark-gluon vertices, we obtain the renormalization graphs of Section 3. If the subdiagram is nested at the effective vertex of the "hard blob" (where four quark lines meet in Figure (1a)), we obtain a sort of ladder structure which is included among the skeleton diagrams of Section 2. Alternatively, Figure (1a) may itself be nested inside an IR divergent diagram, such as Figures (1b) and (1c), at the "hard blob" vertex. This too leads to diagrams of the "ladder" type. Of course, Figures (1b) and (1c) themselves cancel with other diagrams, but, when (a) is nested inside them, non-cancelling diagrams result.

2. Ladder Diagrams

As explained at the end of the last section, all ladder diagrams have nested in them somewhere one of the $\alpha_s^2 \eta^{-1}$ graphs discussed in reference [3]; so it is convenient to define a shortened graphical notation for such diagrams. The sum of all such virtual graphs will be denoted as in Figure (2a), and real graphs as in Figure (2b).

We begin by considering the class of diagrams shown in Figure (3). Here the nesting is according to the ordering of the three-vector magnitudes

$$k''_\ell \ll k''_{\ell-1} \ll \dots k''_1 \quad ; \quad k_m \ll k_{m-1} \ll \dots k_1 \ll k, \bar{k} \ll k'_n \ll \dots k'_1 \tag{11}$$

If we write

$$k = u v \quad ; \quad \bar{k} = u(1-v) \tag{12}$$

then u is controlled by the ordering (11), but v is free. In the nesting approximation, the integrals in Figure (3) almost factorize: the angular integrations and the v-integration completely factorize, and the u-integration and the integrations over the magnitudes of the other three-vectors factorize except that their limits are interrelated by the inequalities (11). A simple example to illustrate this is worked out in Appendix B.

The v-integration and the angular integrations for $\underset{\sim}{k}$ and $\underset{\sim}{\bar{k}}$ give the same function encountered in references [1,...4]:

$$2\alpha^2 \left(\beta^{-1} - 1\right) F(\beta) \tag{13}$$

where F is defined in (8). The angular integration for any of the other $l+m+n$ three-vectors in Figure (3) gives simply

$$\frac{\alpha}{2\pi} \int_{-1}^{1} dx \, \frac{\beta^2(1-x^2)}{(1-\beta x)^2} = \frac{2\alpha}{\pi} F(\beta) \tag{14}$$

The virtual integrations over $k''_1, \dots k''_\ell$ give just the same thing as the real ones, but with opposite sign, since the integrations over k''_{i_0} $(i = 1, \dots l)$ may be done by closing the contour in the

upper-half-space where the only pole is the one from the gluon propagator.

The integrals over the magnitude of the three-momenta and over u give

$$(-1)^{\ell} \int dk''_1 \dots dk''_{\ell}\; dk_1 \dots dk_m\; dk'_1 \dots dk'_n\, du \times \\ \times \left(k''_1 \dots k''_{\ell}\; k_1 \dots k_m\; k'_1 \dots k'_n\right)^{-1+\eta}\; u^{-1+2\eta} \qquad (15)$$

over the region

$$k''_{\ell} < k''_{\ell-1} < \dots < k''_1 < \Delta \quad , \\ k_m < k_{m-1} < \dots < k_1 < u < k'_n < \dots < k'_1 < \Delta \qquad (16)$$

This region is obtained from (11) with the addition of an arbitrary upper-limit Δ which separates "soft" from "hard". Summing (15) over l, m for fixed $l+m = N$, we get

$$(-1)^N \int dk'''_1 \dots dk'''_N\; dk'_1 \dots dk'_n\, du \left(k'''_1 \dots k'''_N\; k'_1 \dots k'_n\right)^{-1+\eta} u^{-1+2\eta} \qquad (17)$$

over $$u < k'_n < \dots k'_1 < \Delta \;;\; u < k'''_N < \dots k'''_1 < \Delta \qquad (18)$$

The integral (17) is equal to

$$(-1)^N \frac{1}{n!}\frac{1}{N!} \int_0^{\Delta} du\; u^{-1+2\eta} \left(\Delta^{\eta} - u^{\eta}\right)^{N+n} \eta^{-N-n} \qquad (19)$$

The colour matrix trace associated with Figure (3) is

$$Tr\{ t_{c_\ell} \dots t_{c_1} t_{c_1} \dots t_{c_\ell}\; t_{a_m} \dots t_{a_1}\; i f_{xyz}\, T_x t_y \times \\ \times\; t_{b_n} \dots t_{b_1}\, H\, t_{b_1} \dots t_{b_n}\; t_z\; t_{a_1} \dots t_{a_m} \} \qquad (20)$$

The first thing to check is that the relationship between the colour matrices in Figure (2b), that was used in references [1...4], is not disturbed by the addicional colour matices in (20). This is so, because the relevant matrices t_y and t_z in (20) are separated in the trace (20) only by a multiple of the unit matrix, because

$$t_c t_c = C_q\, I \qquad (21)$$

where C_q is the Casimir invariant for the representation associated with q. This fact justifies our treating the sum of diagrams in Figure (2b) as a unit.

Introducing the coefficient from (19) in front of (20) we get

$$(-1)^N \frac{1}{n!}\frac{1}{N!}\frac{1}{2} C_G \times$$
$$\times Tr\{t_{a_1}\dots t_{a_N} t_{a_N}\dots t_{a_1}\, t.T\, t_{b_n}\dots t_{b_1} H\, t_{b_1}\dots t_{b_n}\} \quad (22)$$

The sum over n, N for fixed $n+N=M$ gives

$$\frac{1}{M!}\frac{C_G}{2} Tr\{t_{c_1}\dots t_{c_M}[\dots[[t.T, t_{c_M}], t_{c_{M-1}}]\dots t_{c_1}]H\} = \quad (23)$$
$$= -\frac{1}{M!}\left(-\frac{1}{2}C_G\right)^{M+1} Tr\{t.T\, H\}$$

We can now verify (7) for the special case $\alpha_s(q)=\alpha_s(\mu)=\alpha_s$, $\mu=1$. To do this, note that the M-th term in the expansion of the exponential is

$$\frac{1}{M!\,\eta^M}\int_0^\Delta du\; u^{-1+2\eta}\left(\Delta^\eta - u^\eta\right)^M \quad (24)$$

in agreement with (19) and (23). The other factors (up to an overall factor of 2) in (7) are supplied by (13) and M powers of (14).

As mentioned above, there is a check on (23) that it is symmetric under $t \leftrightarrow T$ although the individual terms in (20) are not.

In Figure (3), we have included one set of renormalization graphs: self-energy parts on the external quark lines of the "rainbow" form. To leading order, this set is in fact equivalent to <u>all</u> self-energy parts on the external quark lines. To see this, observe that the leading IR divergences of the rainbow graphs exponentiate to give

$$\exp\left[-\frac{\alpha}{\pi} C_q \frac{1}{\eta} F(\beta)\right] \quad (25)$$

as is clear from the ordering of the k_i'' in (15) and (16), and the t_{c_i} in (20). On the other hand, (25) is known [5] to be the complete leading result from self-energy parts on external lines. The complete contribution is given by the inverse of the function R which is determined by the behaviour of the one-particle irreducible self-energy Σ^* near mass-shell: $\Sigma^*(q) = R(q)(i\not{q} + m)$. The function R is obtained by differentiating Σ^* with respect to the momentum and taking the on-shell matrix elements of the resulting expression. As a consequence of the Ward identities, the set of diagrams contributing to R obtained this way have, to leading order, precisely the "rainbow" structure considered above.

Next we consider Figure (4), which is like Figure (3), except that it contains Figure (2a) not Figure (2b). The reason is firstly that the ordering of the momenta is exactly the same as in (16), and secondly that the angular and v -integration for the sub-graph Figure (2a) gives the same as Figure (2b) with the same sign (see reference [3]). Thus, the contribution from Figure (3) is just doubled, providing the factor 2 in (7).

The final step in this chapter is to show that the addition of further Coulomb exchanges to Figure (3) or (4) does not give leading contributions. Rather than try to draw a general diagram, we consider a typical example in Figure (5), in which the ordering is

$$k_1 < k_2 < k_3 < \left\{ \begin{matrix} k_4 \\ k_5 \end{matrix} \right\} < u < k_6 < \left\{ \begin{matrix} k_7 < k_8 \\ k_9 \end{matrix} \right\} \qquad (26)$$

Apart from the integrals over the magnitudes of the k_i and over u, the diagram factorizes into independent angular integrations in the nesting approximation.

If there were no real gluons emitted, but only the Coulomb exchanges, the right-hand side of the diagram would provide essentially the same IR divergent phase-factor as in QED:

$$\exp\left[\frac{\alpha}{2\pi}\, t.T \int_{-1}^{1} dx \, \frac{\eta^{-1}}{\beta x - i\varepsilon}\right] = \exp\left[i\,\frac{\alpha}{2}\, t.T\, \beta^{-1}\eta^{-1}\right] \qquad (27)$$

(this is true in the ladder approximation and is also, in fact, exact in the pure Coulomb case). This phase-factor is exactly cancelled by its complex-conjugate, which comes from Coulomb exchanges in the left-hand side of the graph.

The point about diagrams like Figure (5) is that essentially the same cancellation occurs, even in the presence of the real gluons. Imagine the real gluon momenta (and u) being held fixed while the Coulomb line integrations are done. Take the blocks of Coulomb momenta in (26), i.e., the block k_1, k_2; the block k_4, k_5; the block k_7, k_8, k_9 , where each block is separated from the

others by a real gluon. Consider the set of graphs generated from Figure (5) by moving the Coulomb lines in any one block from one side of the graph to the other, but keeping them in the same position in (26) relative to the real gluons. For example, there will be graphs in which k_4 and k_5 appear together on the same side of the graph, but always between k_3 and u Then we assert that cancellation takes place within such sets of graphs, just as in the pure Coulomb case. The only differences from the pure Coulomb case (in the ladder approximation) concern the constraints (26) and the order of colour-matrix multiplication. The constraints (26) are irrelevant, since they affect each graph of a set in the same way. As far as colour-matrices go, passing from one graph of a set to another means altering the position of a matrix $t.T$. We can imagine $t.T$ moved to its new position either by passing round the edge of the graph (using the fact that there is a trace) or by passing through the "hard blob" at the center of the graph. In either case, $t.T$ is moved through a product of matrices forming a colour invariant. For example, moving k_5 to the right-hand side of Figure (5), next to k_4, means moving $t.T$ the other side of the product $t_\alpha (t.T)^2 t_\alpha$. If we moved it through the center, we would encounter $t_\alpha t_\beta (t.T)^2 H (t.T) t_\beta t_\alpha$, which is also an invariant since H is invariant. But $(t_a + T_a)$ commutes with any invariant, and so therefore does $t.T$. Thus, $t.T$ can be moved to its new position with no change.

3. Renormalization Graphs

In this section we add, to the ladder graphs of Figure (3), UV divergent sub-graphs (other than the self-energy parts on external quark lines, which we already included in Figure (3)). We argue that these graphs account for the appearance of the running constant in (7). We first give a general argument why this should happen, and then illustrate the detailed mechanism with a few examples of renormalization sub-graphs of order α_s only. Thus the work in this section is by no means rigorous or complete.

The general argument for our claim is as follows. If we use dimensional regularization and minimal substraction [6], every UV divergent graph gives, after substraction, a $\ln\mu$ dependence, where μ is the arbitrary mass unit introduced in the process. This must be the logarithm of the ratio of μ to either a quark mass or to one of the soft gluon momenta. If it is the latter, we get the running coupling constant as in (7). (If the renormalization graph is on one of the lines or vertices of Figure (2), it does not matter whether we have $\ln k$ or $\ln\bar{k}$, since they both scale to zero as $\ln\mu$, which is what appears in (7)).

It remains to try to decide which of the $\ln\mu$ dependence does <u>not</u> appear as $\ln(\mu/m)$ (where m is a quark mass). A plausible answer to this question is that it is the part of the renormalization sub-graphs which depends upon C_G but which is independent of C_f and C_a, since it is this part which occurs in a pure Yang-Mills theory, without any quarks.

We now turn to the examination of a few simple cases. We begin with renormalization graphs associated with the Coulomb lines in Figure (2), since this is much the simplest case. Examples of relevant sub-graphs are shown in Figure (6). The self-energy parts in (6a) provide a factor

$$-\frac{11}{6\pi}\alpha_s C_G \ln\frac{|\underset{\sim}{k}|}{\mu} \tag{28}$$

(k_o is always zero in these graphs, because the contour integration in the lower half-plane picks up the pole at $k_o = 0$, see reference [3]), for it is well-known that for Coulomb lines the self-energy parts give the complete coupling constant renormalization [7].

It is perhaps worthwhile to see how the other graphs in Figure (6) cancel. For fixed, non-zero $|\underset{\sim}{k}|$, the vertex-parts are IR convergent but contain $\ln|\underset{\sim}{k}|$ terms. The coefficient of these terms may be determined by setting $\underset{\sim}{k} = 0$ and finding the consequent IR divergence (for instance, by using dimensional IR regularization with an upper cut-off Δ). It is then easy to check that the C_q parts of (b) and (e) cancel (this is a consequence of the QED Ward identity) and the C_G parts of (b) and (d) cancel. Graph (c) (and the reflected graph) give zero because the vertex is proportional to $|\underset{\sim}{k}|$.

Next we consider the renormalization graphs associated with a real transverse gluon, as in Figure (7). Graphs (c) and (d) are straightforward. They are IR convergent (for $q+k$ off-shell but $k^2 = 0$) and give a contribution

$$\frac{F(\beta)}{\pi}\alpha_s C_G \ln|\underset{\sim}{k}_1| \tag{29}$$

which may be determined by the method used for the Coulomb graphs.

The remaining graphs are more complicated, since they are IR divergent for q on-shell, even for non-zero $|\underset{\sim}{k}|$. However, these IR divergences cancel when (a) and (b) are combined and the sum gives

$$-\frac{3}{12\pi}\alpha_s C_G \ln|\underset{\sim}{k}_1| \tag{30}$$

The same thing happens with graphs (e)...(i). Details are given in Appendix C. The result is a contribution

$$-\frac{1}{\pi}\left[F(\beta)+\frac{2}{3}\right]\alpha_s C_G \ln|\underset{\sim}{k}_1| \qquad (31)$$

Taking into account a factor of 2 which arises when considering also the corrections on the other end of the gluons, we see that expressions (29), (30) and (31) combine to give precisely a similar factor to equation (28).

Thus we have verified the appearance of the running coupling constant in (7), up to one-loop order. Note that the blobs defined in Figure (2) acquire two corrections (28), one from the Coulomb line and one from the transverse line. This is as it should be because $\alpha_s(u)$, corresponding to these subgraphs, occurs squared in (7).

In the foregoing, we have not actually checked the renormalization of the three-gluon vertices in Figure (2). However, we expect them to work out correctly, since no quark mass is involved. This is further supported by an analysis in the axial gauge (see Appendix D) where we can verify the appearance of the running coupling constant to all orders.

4. Discussion

Here we comment on the significance of formula (7), as far as we are able. We emphasize that it is derived in the leading logarithm approximation only, so any inferences from it are only tentative.

For immediate practical purposes, the most important feature of (7) is factor $(\beta^{-1}-1)$ which persists from the α_s^2 calculations [1,...4]. This means that the IR divergences only affect power corrections (higher-twist terms) in high-energy perturbative QCD. It is noteworthy that, within such power correction terms, the running coupling constant α_s appears with a <u>soft</u> argument (u and q in (7)) and not the characteristic hard momentum of the reaction.

In evaluating the integrals in (7), we meet the problem that, in the strict leading logarithm approximation (9), $\alpha_s(q)$ becomes negative for small enough q, which presumably makes no physical sense. We have therefore investigated equation (7) by guessing the true behaviour of $\alpha_s(q)$ as $q \to 0$. This is a rather hybrid approximation, but it is perhaps interesting to see what it gives.

We assume, for concreteness, that

$$\alpha_s(q) = A\, q^{-a} \qquad \text{as} \qquad q \to 0 \tag{32}$$

where $a \geq 0$. We can then set $\eta = 0$ straightaway in equation (7). The integrals are convergent and give

$$2\,\mathrm{Tr}\,(t.T\,H)\,(\beta^{-1}-1)\,\pi\left[\alpha_s(\Delta) + \frac{a\pi}{C_G F(\beta)}\right] \tag{33}$$

a <u>finite</u>, <u>non-zero</u> result.

This expression is essentially non-perturbative. It contains terms of order α_s and 1 (for $a \neq 0$) whereas equation (7) is of order α_s^2. Expression (33) is singular at $\beta = 0$, particularly if $a \neq 0$. This probably indicates that the hybrid leading-logarithm approximation we have used is applicable (if at all) away from $\beta = 0$. It is interesting to remark that, if we rescale $\alpha_s \to C_G^{-1}\alpha_s$, (33) becomes proportional to C_G^{-1}. (Of course, this can also be seen directly from equation (7)) This implies, in particular, that in the large N-limit (in SU(N), $C_G = N$) the corrections expressed by our result become very small.

We are grateful to M.L.Frenkel and P.V.Landshoff for helpful discussions. J.F. acknowledges a grant from Conselho Nacional de Pesquisas (CNPq), and C.E.C. and M.T.T. thank the Fundação de Amparo à Pesquisa do Estado de São Paulo (FAPESP) for financial support.

Appendix A

The purpose of this appendix is to introduce a direct method of calculation, which stresses the reason for the existence of a simple answer for the uncancelled IR divergences. In order to understand how IR divergences can be present in reaction (1), let us compare it with the process:

$$\gamma^* \longrightarrow q + \bar{q} + \text{soft gluons} \qquad \text{(A1)}$$

where the gluons are emitted from outgoing (massive) fermions. As shown in reference (8), the IR divergences in the process cancel out, basically as a simple consequence of unitarity. Given this fact, using the invariance of our theory under time-reversal, we will transform (A1) in the following reaction:

$$q + \bar{q} + \text{soft gluons} \longrightarrow \gamma^* \qquad \text{(A2)}$$

which is more directly related to our process (1). In (A2), again, the IR divergences will cancel, but note that the soft gluons are absorbed by the incoming fermions, as opposite to the reaction (1), where they are emitted. As we will see, this difference is crucial for the existence of uncancelled IR divergences in process (1).

Let us denote the graphs containing the absorbed (real) gluons contributing to reaction (A2) by R^a, and the graphs containing the emitted gluons contributing to (1) by R^e. Furthermore, we denote by V the purely virtual graphs contributing to the "elastic" reaction $q + \bar{q} \rightarrow \gamma^*$. Then, as far as the IR divergences are concerned, we can write:

$$R^a + V = 0 \qquad \text{(A3)}$$

for reaction (A2), whereas for the process (1) we have:

$$R^e + V = D \qquad \text{(A4)}$$

where D denotes the uncancelled IR divergences we are looking for.

Taking the difference between these two equations, we obtain D as follows:

$$R^e - R^a = D \tag{A5}$$

An immediate consequence of this equation is the cancellation of the leading IR divergences. Tosee this, note that R^e differs from R^a by the direction of momenta of the real gluons. Using the eikonal approximation, it is easy to see by direct inspection of the graphs that, by conveniently routing the direction of virtual gluon momenta, R^a can be obtained directly from R^e just by changing the sign of all $i\varepsilon$ in the fermion denominators. As is well known, for the leading IR divergences, we can disregard these $i\varepsilon$, in which case we obtain at once that:

$$(R^e - R^a)^{lead} = D^{lead} = 0 \tag{A6}$$

which holds to all orders in perturbation theory. In particular, this is trivially true in second-order, where all IR divergences are, by definition, leading.

However, for the next-to-leading IR divergences, which appear first in fourth-order, we must be careful when considering the effect of the difference of the sign of $i\varepsilon$ in the fermion propagators in R^e and R^a. Let us illustrate here this effect in fourth-order where, in terms of the group, C_G, and quark, C_q, Casimir numbers, the cross-section has the form:

$$\sigma_{Born}\ T_R(I)\ \{ A\, C_q^2 + D\, C_q C_G \} \tag{A7}$$

The abelian case has $C_G = 0$ and is IR finite, which implies that A must be finite. Therefore, for our purposes, it is sufficient to restrict ourselves to graphs contributing to D.

We begin by considering the abelian graph shown in Figure (8a). For R^e, we perform the k_0-integration in the lower half-plane using Cauchy's theorem, where we encounter poles coming from gluon and quark propagators. Then, dropping the remaining $i\varepsilon$

since we can show that these do not contribute to the cross-sections, we obtain in order:

$$-\frac{1}{4}\frac{(p\cdot q)\,p^2}{(2\pi)^6}\int\frac{d^3k}{|\underset{\sim}{k}|}\frac{d^3k'}{|\underset{\sim}{k}'|}\left\{\frac{1}{2}(p.k)^{-1}[p.(k+k')]^{-1}(p.k')^{-1}(q.k)^{-1}+\right.$$
$$\left.-\frac{1}{q_0 p_0^2}|\underset{\sim}{k}|(p.k')^{-1}\left[\left(\frac{\underset{\sim}{q}\cdot\underset{\sim}{k}}{q_0}\right)^2-|\underset{\sim}{k}|^2\right]^{-1}\left(\frac{\underset{\sim}{q}\cdot\underset{\sim}{k}}{q_0}-\frac{\underset{\sim}{p}\cdot\underset{\sim}{k}}{p_0}\right)^{-1}\left(\frac{\underset{\sim}{q}\cdot\underset{\sim}{k}}{q_0}-\frac{\underset{\sim}{p}\cdot\underset{\sim}{k}}{p_0}-\frac{p.k'}{p_0}\right)^{-1}\right\} \tag{A8}$$

For R^a, which has the sign of $i\varepsilon$ in the fermion denominators opposite, we perform the k_0-integration in the upper half-plane. The contribution from the gluon propagators is the same as above, and cancels in (A5). On the other hand, the contribution coming from the fermion pole has opposite sign, and, consequently, adds in (A5) to the corresponding one in R^e. Since the Feynman gauge is Lorentz invariant, we can calculate these contributions more conveniently in the rest frame of the anti-quark $\underset{\sim}{p}=0$. Adding now also the contributions obtained from Figure (8a) by moving k' to all possible places, we obtain for D_a:

$$D_a = -\frac{2\beta}{(2\pi)^6}\int d^{3+\eta}k\, d^{3+\eta}k'\frac{1}{|\underset{\sim}{k}'|^2}\left(\kappa^2-|\underset{\sim}{k}|^2\right)^{-1}\kappa^{-1}\times$$
$$\times\left(\kappa+|\underset{\sim}{k}'|\right)^{-1}\left(\frac{\cos\theta'}{\beta\cos\theta'-1}\right) \tag{A9}$$

Here θ' denotes the angle between $\underset{\sim}{k}'$ and $\underset{\sim}{q}$ and we have defined $\kappa \equiv q_0^{-1}(\underset{\sim}{q}\cdot\underset{\sim}{k})$. The integration over θ' gives:

$$\int_0^\pi(\sin\theta')^{1+\eta}\frac{\cos\theta'\,d\theta'}{\beta\cos\theta'-1} = -\frac{2}{\beta}\left(\frac{1}{2\beta}\ln\frac{1+\beta}{1-\beta}-1\right)+O(\eta) \tag{A10a}$$

Introducing new variables u and v via $k=\frac{u\Delta}{1+v}$, $k'=\frac{\beta uv\Delta}{1+v}$, we perform the rest of the integration which gives, in addition to a factor proportional to β^{-1}, the IR divergence:

$$\int_0^1\frac{du}{u}\,u^{2\eta} = \frac{1}{2\eta} \tag{A10b}$$

Together with (A10a), we then see that (A9) leads to

$$D_a = \frac{1}{8\pi^2}\frac{1}{\beta}F(\beta)\frac{1}{2\eta} \tag{A11}$$

where $F(\beta)$ is the bremsstrahlung function defined in (8).

We now consider the contributions to D, coming via (A5) from the non-abelian graphs shown in Figure (8b). After a little calculation, we obtain:

$$-\frac{1}{2}\frac{1}{(2\pi)^6}\int d^{4+\eta}k\;\frac{d^{3+\eta}k'}{|\underset{\sim}{k}'|}\left[q^2 p-(p\cdot q)q\right]\cdot(k-k')\;\frac{1}{q\cdot k'}\;\times$$

$$\times\left\{\frac{1}{k^2}\;\frac{1}{(k+k')^2}\;-\pi^2\delta(k^2)\,\delta\left[(k+k')^2\right]\right\}\left\{\frac{\delta(q\cdot k)}{p\cdot(k+k')}-\frac{\delta\left[p\cdot(k+k')\right]}{q\cdot k}\right\} \qquad \text{(A12)}$$

Here, the δ -functions in the first bracket arise from the $i\varepsilon$ present in the gluon propagators, and it can be shown that, in the dimensional regularization scheme, these functions will not actually contribute to the cross-section. The δ -functions present in the second bracket arise from the $i\varepsilon$ present in the fermion denominators.

Similarly, for the contribution to D coming from the non-abelian graph in Figure (8c), we obtain the result:

$$\frac{1}{2}\;\frac{1}{(2\pi)^6}\int d^{4+\eta}k\;\frac{d^{3+\eta}k'}{|\underset{\sim}{k}'|}\left[p^2 q-(p\cdot q)p\right]\cdot(2k+k')\;\times \qquad \text{(A13)}$$

$$\times\;\frac{1}{k^2}\;\frac{1}{(k+k')^2}\;\frac{1}{p\cdot k'}\;\frac{1}{q\cdot k'}\;\delta(p\cdot k)$$

We will now perform the k_o -integrations in equations (A12) and (A13) with the help of the δ -functions. Since each term involving these functions is separately Lorentz invariant, for convenience, we have calculated these terms in a suitable frame of reference.

For the first term in (A12) involving $\delta(q\cdot k)$, we use the rest frame of the quark $\underset{\sim}{q}=0$. After performing the k_o -integration, we make $\underset{\sim}{k}'\to\underset{\sim}{k}'-\underset{\sim}{k}$ and then symmetrize under $\underset{\sim}{k}\,,\underset{\sim}{k}'\to-\underset{\sim}{k}\,,-\underset{\sim}{k}'$. Next we perform angular integrations, using the system of angular coordinates described in the Appendix of reference [3]. We obtain (for simplicity of notation we put $|\underset{\sim}{k}|=k$; $|\underset{\sim}{k}'|=k'$ and $\cos\Theta'=x'$) :

$$-\frac{1}{2}\frac{1}{(2\pi)^6}(2\pi)^2\int_0^{\Delta}\frac{dk}{k}\int_0^{\Delta}\frac{dk'}{k'}(kk')^{\eta}\int_0^{1}dx'\left\{\frac{k'^2-k^2}{k'^2}\left(\ln\left|\frac{k-2k'}{k+2k'}\right|\right)\frac{1}{1-\beta^2x'^2}\times\right.$$

$$\left.\times\left(1-\frac{1}{1-\beta^2x'^2}\,\frac{k'^2-k^2}{k'^2}\right)\left(\ln\left|\frac{(k-k')^2-\beta^2k'^2x'^2}{(k+k')^2-\beta^2k'^2x'^2}\right|\right)-(\beta=0)\right\} \qquad \text{(A14a)}$$

Making now the change of variables: $k=\frac{\Delta u v}{1+v}$, $k'=\frac{\Delta u}{1+v}$ we obtain after some calculation:

$$-\frac{1}{2}\frac{1}{(2\pi)^6}\,\frac{(2\pi)^4}{8}\,\frac{1}{2\eta}\left[\frac{1}{2\beta}\left(\ln\frac{1+\beta}{1-\beta}\right)-1\right] \qquad \text{(A14b)}$$

Consider now the part involving the $\delta[p.(k+k')]$ function in (A12) and perform the k_o-integration, using the rest frame of the anti-quark $\underset{\sim}{p}=0$. Symmetrizing under the transformation $\underset{\sim}{k}$, $\underset{\sim}{k}'\to-\underset{\sim}{k}$, $-\underset{\sim}{k}'$, after a little calculation, we obtain:

$$-\frac{1}{2}\frac{1}{(2\pi)^6}\int d^{3+\eta}k\;d^{3+\eta}k'\,\frac{1}{(k+k')^2}\left(2\beta^2\kappa+\kappa-\kappa'\right)\times$$

$$\times\left(\kappa+\kappa'\right)^{-1}\left(k^2-\kappa^2\right)^{-1}\left(k'^2-\kappa^2\right)^{-1} \qquad \text{(A15a)}$$

But this contribution, apart from an overall constant factor, is precisely the same as equation $\{(25)+(26)\}$ of reference [1]. This has been evaluated explicitly in the Appendix of reference [3]. Using this fact, we obtain:

$$-\frac{1}{2}\frac{1}{(2\pi)^6}\,\frac{(2\pi)^4}{4}\,\frac{1}{2\eta}\left[\frac{1}{2\beta}\left(\ln\frac{1+\beta}{1-\beta}\right)-1\right] \qquad \text{(A15b)}$$

Consider finally equation (A13) and perform, with the help of the δ-function, the k_o-integration in the rest frame of the anti-quark: $\underset{\sim}{p}=o$. Using the same system of angular coordinates as employed in (A14a), we perform angular integrations and obtain:

$$\frac{1}{(2\pi)^6}\left[\frac{1}{2\beta}\left(\ln\frac{1+\beta}{1-\beta}\right)-1\right]\int_0^{\Delta}\frac{dk}{k}\int_0^{\Delta}\frac{dk'}{k'}(kk')^{\eta}\int_0^{\pi}\sin\psi\,d\psi\,\frac{k'+2k\cos\psi}{k+2k'\cos\psi} \qquad \text{(A16a)}$$

where ψ denotes the angle between $\underset{\sim}{k}$ and $\underset{\sim}{k}'$. We now symmetrize explicitly under $\cos\psi\to-\cos\psi$ and perform the k'-integration. Then we define newvariables u and v via: $k=\frac{\Delta u}{1+v}$ and $\cos\psi=\frac{uv}{2(1+v)}$

Integrating over u and v, we obtain for the part containing the IR divergence the result:

$$\frac{1}{2}\,\frac{1}{(2\pi)^6}\,\frac{(2\pi)^4}{8}\,\frac{1}{2\eta}\left[\frac{1}{2\beta}\left(\ln\frac{1+\beta}{1-\beta}\right)-1\right] \qquad \text{(A16b)}$$

Adding now (A14b), (A15b) and (A16b), and considering also the graphs obtained by exchanging $p \leftrightarrow q$ in the diagrams considered above, we obtain for the contributions resulting from the non-abelian graphs:

$$D_{n.a} = \frac{1}{8\pi^2}\,(-1)\,F(\beta)\,\frac{1}{2\eta} \qquad \text{(A17)}$$

We remark that there are also other graphs contributing equally to R^e and R^a, so that their contributions cancel in equation (A5). For instance, consider the fourth-order diagram containing a self-energy insertion on the (external) gluon line. In this case, due to the fact that the self-energy is an even function of the external momenta, it is easy to see that $R^e = R^a$ and therefore, these graphs will not contribute to this order, Adding equations (A11) and (A17), we find a simple result for the uncancelled IR divergences present to fourth-order:

$$\sigma_{Born}\;Tr(I)\;2\,C_q\,C_G\left(\frac{1}{\beta}-1\right)F(\beta)\,\frac{1}{2\eta}\,\alpha_s^2 \qquad \text{(A18)}$$

Basically this result arises as follows: after the cancellation of the leading IR divergences in $R^e - R^a$, we are left with the non-leading contributions in R^e which have opposite signs to the corresponding ones in R^a. Consequently, these contributions effectively add in $R^e - R^a$, so that the uncancelled non-leading IR result comes essentially from R^e. But, R^e represents the cross-section for the emission of a real gluon, and precisely for this reason, our answer is proportional to the bremsstrahlung probability function.

Appendix B

In this appendix we demonstrate that "nesting" works for Figure (1d) by explicit calculation.

Figure (1d) gives a contribution (after integrating over the time-component of the Coulomb propagator)

$$\alpha \int_{-1}^{1} dx\, dx_1\, dx_2 \frac{(1-x_1^2)(1-x_2^2)}{(x\beta + i\varepsilon)(x_1\beta - 1 - i\varepsilon)} \times \tag{B1}$$

$$\times \int_{k}^{\Delta} dk\, dk_1\, dk_2 \frac{k^{\eta-1} k_1^{\eta} k_2^{\eta+1}}{(k + k_1 - k_1 + i\varepsilon)(k + k_1 + k_2 - k_1 - k_2 + i\varepsilon)(k_1 + k_2 - k_1 - k_2 - i\varepsilon)}$$

where

$$\alpha = 2\,\sigma_{Born}\,\alpha_s^3 \sum_{abc} Tr(T_a t_c t_b t_a t_b t_c)$$

We have used polar coordinates and dimensional regularization ($d = 3 + \eta$). Further, since we are concerned only with leading IR divergences, we can ignore the effect of dimensional regularization on the angular integrations.

Since our quarks are massive, we can make the change of variables: $k_1 \to k_1 (1 - x_1\beta)^{-1}$; $k_2 \to k_2 (1 - x_2\beta)^{-1}$ under which (B1) becomes

$$\alpha \int_{-1}^{1} \frac{dx\, dx_1\, dx_2 (1-x_1^2)(1-x_2^2)}{(x\beta + i\varepsilon)(1 - x_1\beta)^2 (1 - x_2\beta)^2} \int_{k}^{\Delta} \frac{dk\, dk_1 dk_2\; k^{\eta-1} k_1^{\eta} k_2^{\eta+1}}{(x\beta k - k_1 + i\varepsilon)(x\beta k - k_1 - k_2 + i\varepsilon)(k_1 + k_2)} \tag{B2}$$

where we have neglected those $i\varepsilon$'s that we may safely do so. With the notation

$$k = u\, w\, v \;; \quad k_1 = u\, w (1 - v); \quad k_2 = u (1 - w) \tag{B3}$$

(which has the Jacobian $u^2 w$) the radial integrations become

$$\int_0^{\Delta} du\, u^{3\eta-1} \int_0^1 dv\, \frac{v^{\eta-1}(1-v)^{\eta}}{vx\beta - 1 + v + i\varepsilon} \int_0^1 \frac{dw\; w^{2\eta-1} (1-w)^{1+\eta}}{(wvx\beta + wv - 1 + i\varepsilon)(1 - wv)} \tag{B4}$$

Expanding $(1 - w)^{1+\eta}$ and retaining divergent terms (when $\eta = 0$) only, the w-integration becomes

$$\int_0^1 dw \frac{w^{2\eta-1}}{(wvx\beta + wv - 1 + i\varepsilon)(1 - wv)} \tag{B5}$$

This integral may be evaluated, to yield

$$-\frac{1}{2\eta} + O(\eta) \tag{B6}$$

Hence, the leading IR divergence of the graph is

$$\alpha\int_{-1}^{1}\frac{dx\,dx_1\,dx_2\,(1-x_1^2)(1-x_2^2)}{(x\beta+i\varepsilon)(1-x_1\beta)^2(1-x_2\beta)^2}\left(\frac{\Delta^{3\eta}}{3\eta}\right)\frac{1}{2\eta}\int_0^1\frac{dv\;v^{\eta-1}(1-v)^{\eta}}{v(x\beta+i\varepsilon)+v-1} \tag{B7}$$

Now consider the "nesting" hypothesis. For this graph, the hypothesis asserts that the leading IR divergence is contained within the region of integration for which $k_2 >> k, k_1$. The contribution from (B2) for this region is

$$-\alpha\int_{-1}^{1}\frac{dx\,dx_1\,dx_2\,(1-x_1^2)(1-x_2^2)}{(x\beta+i\varepsilon)(1-x_1\beta)^2(1-x_2\beta)^2}\int_0^{\Delta}dk_2\,k_2^{\eta-1}\int_0^{k,k_1\ll k_2}\frac{dk\,dk_1\;k^{\eta-1}\,k_1^{\eta}}{x\beta k-k_1+i\varepsilon} \tag{B8}$$

With the notation $k=\mu v$; $k_1=\mu(1-v)$ (which has the Jacobian μ) the integral over k, k_1 becomes

$$\int_0^{ak_2}d\mu\;\mu^{2\eta-1}\int_0^1\frac{dv\;v^{\eta-1}(1-v)^{\eta}}{x\beta v+v-1+i\varepsilon} \tag{B9}$$

where a is some (arbitrary) constant ($<< 1$) used to implement the restriction $k_2 >> k, k_1$. Hence (B8) is

$$-\alpha\int_{-1}^{1}\frac{dx\,dx_1\,dx_2\,(1-x_1^2)(1-x_2^2)}{(x\beta+i\varepsilon)(1-x_1\beta)^2(1-x_2\beta)^2}\int_0^{\Delta}dk_2\,k_1^{3\eta-1}\;\frac{a^{2\eta}}{2\eta}\int_0^1\frac{dv\;v^{\eta-1}(1-v)^{\eta}}{x\beta v+v-1+i\varepsilon} \tag{B10}$$

However

$$a^{2\eta} = 1 + 2\eta\,\ln a + O(\eta) \tag{B11}$$

so the leading IR divergence of (B8) is the same as (B7), and does not contain the arbitrary constant a.

Appendix C

Here we illustrate the ideas of Section 3 on renormalization graphs, considering in detail the graphs of Figure (7c...i)

For simplicity, we will introduce the integral operator A_{a_i}, corresponding to the graph in Figure (1a) with the understanding that whatever it acts on replaces a p_i within the integrand of the two-loop integrations (which we will denote by k and k_1). Further, it will be understood that any extra colour structure in the operand replaces either of the t_a's in the trace of the colour matrices, which is then summed over repeated indices, as usual.

Thus, we write the contribution from Figure (7c) as (after integrating over k_2° by Cauchy):

$$A_{a_i}[t_b t_a t_b]\frac{g^2}{(2\pi)^3}\int \frac{d^3k_2}{2k_2}\ \frac{p_i\beta^2(1-x_2^2)}{(\kappa_2-k_2-i\varepsilon)(\kappa_1+\kappa_2-k_1-k_2-i\varepsilon)} \qquad (C1)$$

In a similar manner Figure (7g) yields

$$-iA_{a_i}[f_{abc}t_b t_c]\frac{g^2}{(2\pi)^3}\int\frac{d^3k_2}{2k_2}\ \frac{\delta^{tr}_{ij}(k_2)\ p_j(k_1+k_2)}{(\kappa_2-k_2-i\varepsilon)(\underset{\sim}{k}_1-\underset{\sim}{k}_2)^2} \qquad (C2)$$

and Figure (7f)

$$-iA_{a_i}[f_{abc}t_b t_c]\frac{g^2}{(2\pi)^3}\int\frac{d^3k_2}{2k_2}\ \frac{\delta^{tr}_{ij}(k_2)\,p_j(k_2-k_1)}{(\kappa_1+\kappa_2-k_1-k_2-i\varepsilon)(\underset{\sim}{k}_1+\underset{\sim}{k}_2)^2} \qquad (C3)$$

Next consider Figure (7d). This must first be renormalized, as renormalization of this sort of graph introduces further IR divergences. We use mass-shell substraction to obtain a contribution

$$-A_{a_i}[t_a t_b t_b]\frac{g^2}{(2\pi)^3}\int\frac{d^3k_2}{2k_2}\ \frac{p_i\beta^2(1-x_2^2)}{(\kappa_2-k_2-i\varepsilon)(\kappa_1+\kappa_2-k_1-k_2-i\varepsilon)} \qquad (C4)$$

This combines with (C1) to yield

$$iA_{a_i}[f_{abc}t_b t_c]\frac{g^2}{(2\pi)^3}\int\frac{d^3k_2}{2k_2}\ \frac{p_i\beta^2(1-x_2)^2}{(\kappa_2-k_2-i\varepsilon)(k_1+\kappa_2-k_1-k_2-i\varepsilon)} \qquad (C5)$$

which has the same colour structure as the other terms.

Figure (7e) has a contribution

$$A_{a_i}[f_{abc}t_b t_c]\frac{g^2}{(2\pi)^4}\int\frac{d^4k_2}{(k_2^2-i\varepsilon)}\;\frac{N_i(k_1,k_2)}{(\kappa_2-k_2^\circ-i\varepsilon)\,[(k_1-k_2)^2-i\varepsilon]} \qquad (C6a)$$

where

$$p_\circ N_i = \delta^{tr}_{jk}(k_2)\,\delta^{tr}_{lm}(k_2-k_1)\,p_k p_m\left[\delta_{ij}(k_1+k_2)_l+\delta_{jl}(k_1-2k_2)+\delta_{li}(k_2-2k_1)_j\right] \qquad (C6b)$$

Since , we can put

$$N_i \equiv A(k_1,k_2)\,p_i + B(k_1,k_2)\,k_1^i = \qquad (C6c)$$

$$=2p_i\left[\frac{\kappa_2\;\underset{\sim}{k}_1\cdot\underset{\sim}{k}_2}{\underset{\sim}{k}_2^{\,2}}-\frac{(\kappa_1-\kappa_2)\,\underset{\sim}{k}_1\cdot(\underset{\sim}{k}_1-\underset{\sim}{k}_2)}{(\underset{\sim}{k}_1-\underset{\sim}{k}_2)^2}\right]+2p_\circ k_2^i\left[\frac{\kappa_2(\kappa_1-\kappa_2)\,\underset{\sim}{k}_2\cdot(\underset{\sim}{k}_1-\underset{\sim}{k}_2)}{\underset{\sim}{k}_2^{\,2}\,(\underset{\sim}{k}_1-\underset{\sim}{k}_2)^2}-\beta^2\right]$$

The k_2° -integration is done by Cauchy (in the upper-half plane). There are two poles, one from each gluon propagator. That due to the $(k_2^2-i\varepsilon)$ propagator leads to an IR divergent integral for that part of the numerator proportional to p_i.

However, Figure (7h) has a contribution (after rearranging the trace of the colour matrices)

$$-iA_{a_i}[-f_{abc}t_b t_c]\frac{g^2}{(2\pi)^3}\int\frac{d^3k_2}{2k_2}\;\frac{1}{2k_1k_2(1-\cos\psi+i\varepsilon)}\;\times$$

$$\times\;\frac{(\kappa+\kappa_1-k_1+i\varepsilon)(\kappa_1-k_1-i\varepsilon)\;N_i(k_1-k_2)}{(\kappa+\kappa_1+\kappa_2-k_1-k_2+i\varepsilon)(\kappa_1+\kappa_2-k_1-k_2-i\varepsilon)(\kappa_2-k_2-i\varepsilon)} \qquad (C7)$$

This has also an IR divergence for that part of the numerator proportional to p_i. Together these two divergent integals yield something of the form $\int dk_2\,k_2^{-1}F(k_2)$ where $F(0)=0$, i.e., the two divergences cancel each other.

We note here that the diagram shown in Figure (7i) does not contribute to the leading IR divergences. The sum of all graphs in Figure (7), then, is IR finite, but may contribute to the leading divergence if there are any $\ln k_1$ terms. We argue that since

$$\frac{1}{\eta}\left(k_1^\eta-1\right)=\ln k_1+O(\eta)$$

if we set $k_1 = 0$ in our expressions after extending the k_2 -integrations to $d = 3+\eta$ spatial dimensions, the coefficient of η^{-1} will be minus that of $\ln k_1$, at least to leading order.

(C2) and (C3) then both yield

$$-iA_{a_i}[f_{abc}t_b t_c]\frac{g^2}{(2\pi)^3}\int\frac{d^d k_2}{2k_2^2}\;\frac{\delta_{ij}^{tr}(k_2)\,p_j}{(\kappa_2 - k_2 - i\epsilon)} \qquad \text{(C8a)}$$

The integral over k_2 must be of the form: (scalar function of p_μ) p_i so we can replace (C8a) with

$$-iA_{a_i}[f_{abc}t_b t_c]\frac{g^2}{(2\pi)^3}\;\frac{p_i}{p^2}\;\int\frac{d^d k_2}{2k_2^2}\;\frac{p_j p_k\,\delta_{jk}^{tr}(k_2)}{(\kappa_2 - k_2 - i\epsilon)} \qquad \text{(C8b)}$$

Using polar coordinates and retaining only η^{-1} terms, this is

$$-iA_{a_i}[f_{abc}t_b t_c]\frac{g^2}{(2\pi)^2}\,p_i\,\frac{1}{\eta}\int_{-1}^{1}dx_2\;\frac{1-x_2^2}{2(x_2\beta - 1)} \qquad \text{(C9)}$$

In a similar manner, (C5) becomes

$$iA_{a_i}[f_{abc}t_b t_c]\frac{g^2}{(2\pi)^2}\,p_i\,\frac{1}{\eta}\int_{-1}^{1}dx_2\;\frac{(1-x_2^2)\beta^2}{2(x_2\beta - 1)^2} \qquad \text{(C10a)}$$

which we integrate by parts

$$iA_{a_i}[f_{abc}t_b t_c]\frac{g^2}{(2\pi)^2}\,p_i\,\frac{1}{\eta}\int_{-1}^{1}dx_2\;\frac{(-2x_2)\beta}{2(x_2\beta - 1)} \qquad \text{(C10b)}$$

Lastly we must deal with Figures (7e) and (7h). The two IR divergent terms are both seen to be zero when $k_1 = 0$, due to the numerator (paying careful attention to the k_1 in the denominator). The remaining term from (7h) does not contribute to the leading divergence. To see this, we write this term out in full, dropping what $i\epsilon$'s we may

$$\sim\int\frac{d^3k\,d^3k_1\,d^3k_2\;\;\delta_{ij}^{tr}(k_1)\;p_i\;k_2^j\;B(k_1,k_2)}{k^2k_1^2k_2^2(1-\cos\psi)(\kappa+i\epsilon)(\kappa+\kappa_1+\kappa_2-k_1-k_2+i\epsilon)(\kappa_1+\kappa_2-k_1-k_2)(\kappa_2-k_2)} \qquad \text{(C11a)}$$

We symmetrize on $k \longrightarrow -k$ and take the real part, obtainig

$$\int^{\Delta}\frac{d^3k\,d^3k_1\,d^3k_2\;\;\delta_{ij}^{tr}(k_1)\;p_i\;k_2^j\;B(k_1,k_2)}{k^2k_1^2k_2^2(1-\cos\psi)\left[(\kappa+i\epsilon)^2-(\kappa_1+\kappa_2-k_1-k_2)^2\right](\kappa_1-k_2)(\kappa_1+\kappa_2-k_1-k_2)} \qquad \text{(C11b)}$$

Since we are considering massive quarks, we can make the change of variables: $k_1(1-x_1\beta)\to k_1$; $k_2(1-x_2\beta)\to k_2$ to perform the radial integrations (in which the leading IR divergence from the graph is to be found) after dimensional regularization, which give

$$\int^{\Delta} \frac{dk\,dk_1\,dk_2\;(k\,k_1\,k_2)^{\eta}}{[(x\beta+i\varepsilon)^2k^2-(k_1+k_2)^2](k_1+k_2)} \qquad \text{(C11c)}$$

with the notation $k=u(1-w)$; $k_1=uw(1-v)$ and $k_2=uvw$ (which has the Jacobean u^2w) this becomes

$$\int_0^{\Delta} du\; u^{3\eta-1}\int_0^1 dv\,dw\,\frac{[v(1-v)w^2(1-w)]^{\eta}}{(x\beta+i\varepsilon)^2(1-w)-w^2} \qquad \text{(C11d)}$$

This is $O(\eta^{-1})$ and so does not contribute to the leading divergence (which is $O(\eta^{-2})$). This leaves us with just the following term from (7e)

$$A_{a_i}[f_{abc}t_bt_c]\frac{g^2}{(2\pi)^4}\,\frac{p_i}{p^2}\int\frac{d^4k_2\;(p\cdot k_2)\,B(k_1=0;k_2)}{(\kappa_2-k_2^{\circ}-i\varepsilon)(k_2^2-i\varepsilon)^2} \qquad \text{(C12a)}$$

The k_2°-integration is evaluated by Cauchy (notice the double pole) in the lower half-plane as usual. Then in polar coordinates and after dimensional regularization, the leading divergence is

$$iA_{a_i}[f_{abc}t_bt_c]\frac{g^2}{(2\pi)^2}p_i\,\frac{1}{\eta}\int\frac{dx_2\;x_2\beta\,(x_2^2-1)(2-x_2\beta)}{2(x_2\beta-1)^2} \qquad \text{(C12b)}$$

integrated by parts gives

$$iA_{a_i}[f_{abc}t_bt_c]\frac{g^2}{(2\pi)^2}\,p_i\,\frac{1}{\eta}\int_{-1}^{1}dx_2\;\frac{-2+2\beta x_2+6x_2^2-4\beta x_2^3}{2(x_2\beta-1)} \qquad \text{(C12c)}$$

The total contribution to the coefficient of $\ln k_1$, resulting from the graphs of Figures (7c)...(7i) is therefore

$$-iA_{a_i}[f_{abc}t_bt_c]\,g^2\,p_i\frac{1}{(2\pi)^2}\int_{-1}^{1}dx_2\,\frac{2x_2^2-2\beta x_2^3}{x_2\beta-1}=$$

$$=\left(A_{a_i}[t_a]\,p_i\right)\left(-\frac{2}{3\pi}\,\alpha_s\,C_G\right) \qquad \text{(C13)}$$

Appendix D

In this appendix we wish to present an analysis which supports the appearance of the running coupling constant in (7) to all orders in perturbation theory. We will restrict ourselves to the factor multiplying the exponential function. To this end, we will use the axial gauge [9], where the Ward identities are simpler, which allows us to simplify the analysis. Of course, the corrections represented by equation (7) should be gauge invariant, and, indeed, using the methods described in appendix A, we have checked explicitly in this gauge that the same answer (A18) is obtained.

The axial gauge is characterized by the gauge condition $n_\mu A^a_\mu = 0$, where n_μ denotes a fixed four vector. In this gauge, the free gluon propagator is

$$D^0_{\mu\nu}(k) = \frac{1}{k^2 - i\varepsilon}\left[\delta_{\mu\nu} - \frac{n_\mu k_\nu + n_\nu k_\mu}{n.k} + \frac{n^2 k_\mu k_\nu}{(n.k)^2}\right] \qquad (D1)$$

Due to the absence of ghosts, the Ward identities are simple, being similar to those encountered in QED. In particular, the quark-gluon-quark irreducible vertex $\Gamma_\lambda(k', p)$ obeys the Ward identity

$$k'_\lambda \Gamma_\lambda(k', p) = \Sigma(k'+p) - \Sigma(p) \qquad (D2)$$

where Σ denotes the self-energy of the quark. Furthermore, the irreducible three-gluon vertex $\Gamma_{\alpha\beta\gamma}(k', k)$ satisfies the Ward identity

$$k'_\alpha \Gamma_{\alpha\beta\gamma}(k', k) = \Pi_{\beta\gamma}(k'+k) - \Pi_{\beta\gamma}(k) \qquad (D3)$$

where $\Pi_{\beta\gamma}$ represents the gluon two-point function.

Consider now the diagrams represented in Figures (9a) and (9b), which represent the effect of the inclusion of vertex and self-energy corrections to the "bare" graphs shown in Figures (8a) and (8b). Diagram (9c) denotes the quark-gluon vertex. As a consequence of the Ward identity (D2), the IR divergences in the graphs

on the right-hand side will cancel, like it happens in QED. Of course, this type of cancellation occurs in all orders, since (D2) is valid to all orders. Similarly, as a consequence of the Ward identity (D3), the IR divergences present in the three-gluon vertex shown in Figure (9d) will cancel at least to leading order.

Thus, we are finally left to consider the gluon self-energy function. To leading order, it is given by the sum of the geometric series shown in Figure(9e). With the help of (D1) it is easy to verify that the leading contribution is given by

$$D^{\ell}_{\mu\nu} = D^{\circ}_{\mu\nu} + D^{\circ}_{\mu\alpha}\, \Pi^{r}_{\alpha\beta}\, D^{\circ}_{\beta\nu} + \ldots = D^{\circ}_{\mu\nu}\,[1-\Pi]^{-1} \qquad \text{(D4)}$$

Here the function Π is determined by the relevant part of the renormalized one-loop gluon self-energy

$$\Pi^{r}_{\alpha\beta}(k) = \Pi\,(\delta_{\alpha\beta}\,k^2 - k_\alpha k_\beta) \qquad \text{(D5a)}$$

with $$\Pi = \frac{-11}{6\pi}\,\alpha_s\, C_G\, \frac{1}{\eta}\left[\left(\frac{k}{\mu}\right)^{\eta} - 1\right] \qquad \text{(D5b)}$$

With the help of this relation, we observe that the bracket in (D4) leads precisely to the leading-logarithm approximation of the running coupling constant defined in (9).

Of course, similar corrections arising from the gluon self-energy occur also on the gluon line k', which is scaled to zero together with k by a common factor u. Therefore, the net effect of the leading corrections is to replace the factor

$$\frac{1}{2\eta}\,\alpha_s^{\,2} = \int_0^{\Delta} du\; u^{-1+2\eta}\,\alpha_s^{\,2} + O(\eta) \qquad \text{(D6)}$$

occuring in (A18) by

$$\int_0^{\Delta} du\; u^{-1+2\eta}\;\alpha_s^{\,2}(u) \qquad \text{(D7)}$$

which gives precisely the coefficient of the exponential occuring in equation (7).

References

[1] R.Doria, J.Frenkel and J.C.Taylor, Nucl. Phys. B168 (1980) 93.

[2] A.Andrasi, C.Carneiro, M.Day, R.Doria, J.Frenkel, J.C.Taylor and M.Thomaz, "Infrared Divergences in Quantum Chromodynamics", to be published in the Proceedings of the XX International Conference on High Energy Physics, Madison, USA (1980).

[3] A.Andrasi, M.Day, R.Doria, J.Frenkel and J.C.Taylor, Oxford University Preprint 37/80 (1980)

[4] C.Di'Lieto, S.Gendron, I.G.Halliday and C.T.Sachrajda, Imperial College and Southampton University Preprint ICTP/79-80/47 - SHEP 79/80-6 (1980).

[5] J.Frenkel, Phys. Lett. 65B (1976) 383.

[6] G.'t Hooft and M.Veltman, Nucl. Phys, B44 (1972) 189; G.'t Hooft, Nucl. Phys. B61 (1973) 455.

[7] I.B.Khriplovich, Sov. J. Nucl. Phys. 10 (1970) 235; J.Frenkel and J.C.Taylor, Nucl. Phys. B109 (1976) 439.

[8] T.Applequist, J.Carrazone, H.Kluberg-Stern and M.Roth, Phys. Rev. Lett. 36 (1976) 768.

[9] W.Konetschny and W.Kummer, Nucl. Phys. B100 (1975) 106; J.Frenkel, Phys. Rev. D13 (1976) 2325.

Figure Captions

Fig.1 a) Prototype non-leading IR divergent diagram of order $\alpha_s^2 \eta^{-1}$. To obtain the uncancelled divergence k and k_1 are scaled to zero together - neither is nested inside the other; b) and c) are IR divergent graphs which may be combined with a) by nesting; d) Example of diagram obtained by nesting b) inside a).

Fig.2 Shortened notation for α_s^2. For the real graphs (b) the real gluon is absorbed somewhere on the other side of the graph.

Fig.3 A class of diagrams of the "ladder" type. Diagrams in which the virtual gluons k_i'' ($i = 1, \ldots 1$) appear on the right should also be included, but this just cancels the factor $\frac{1}{2}$ associated with the self-energy part on an external line. The hermitian conjugate should also be added (i.e., the mirror image of the above graph).

Fig.4 The skeleton diagrams are like Figure (3) but with Figure (2b) replaced by Figure (2a).

Fig.5 Typical example of skeleton graph, containing Coulomb exchanges, whose leading IR divergences cancel when taken together with other graphs with the Coulomb lines in different places.

Fig.6 Examples of renormalization graphs associated with the Coulomb line. The black box in a) includes all second-order self-energy parts constructed from Coulomb and transverse gluons lines.

Fig.7 Renormalization graphs associated with a real gluon. The gluon lines with small circles at their ends are supposed to be attached to a quark line on the other side of the graph.

Fig.8 Example of diagrams which contribute in the Feynman gauge via (A5) to process (1). The small circles represent the emission of the virtual photon. The right-hand graphs denote the complex conjugate of the left-hand ones, and the corresponding complex conjugate diagrams are also to be added.

Fig.9 a) and b) Example of diagrams contributing in the axial gauge to the factor multiplying the exponential in (7); c) represents the quark-gluon vertex, while d) denotes the three-gluon vertex. Diagram d) defines the gluon self-energy, which leads to the appearance of the running coupling constant.

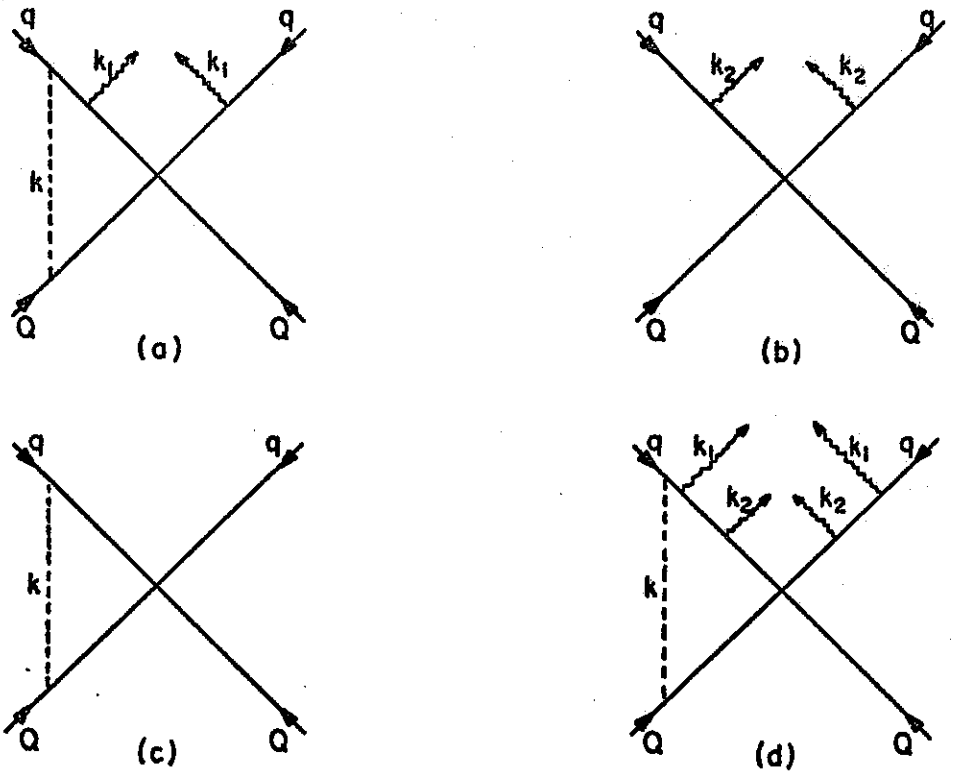

Figure 1

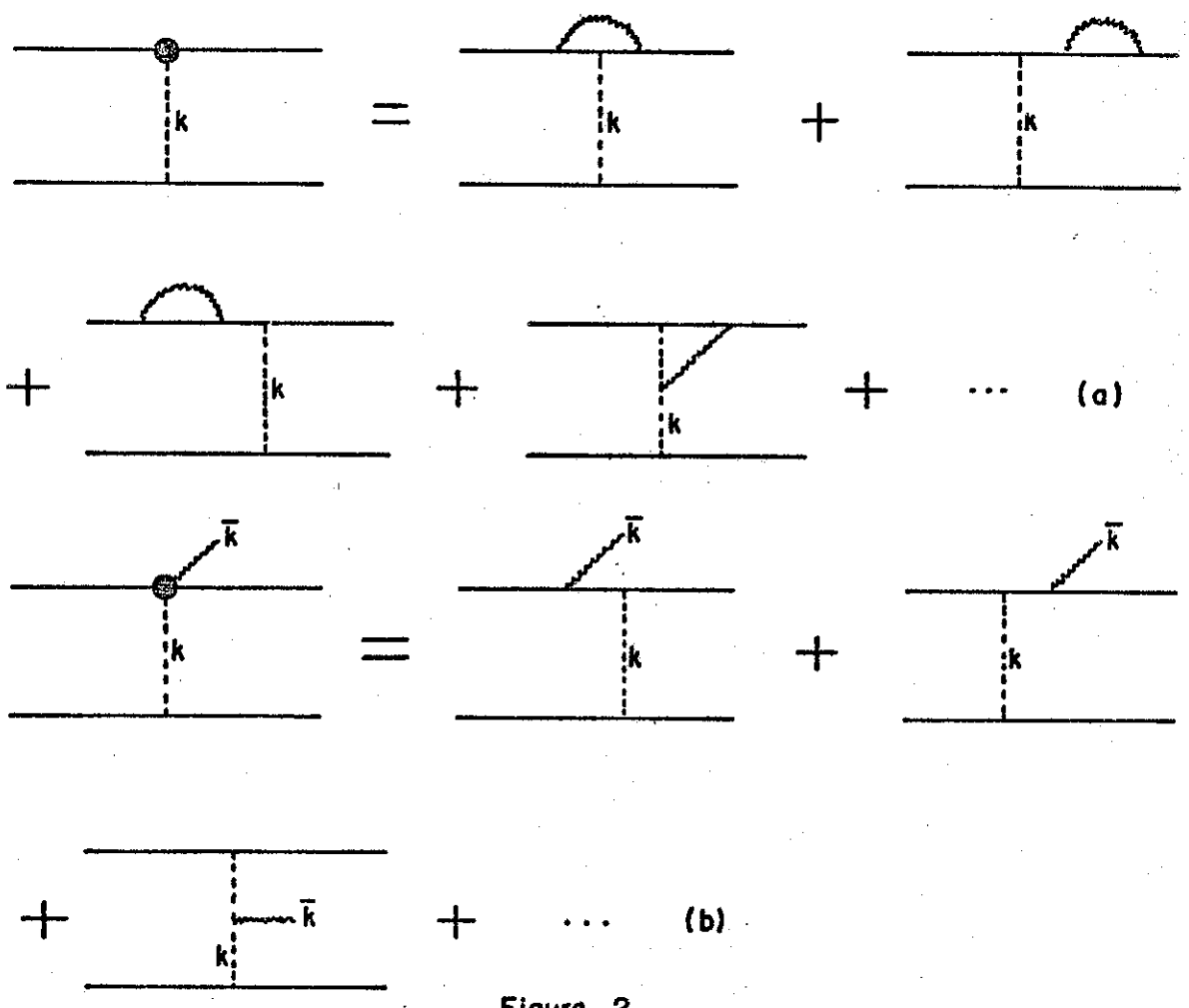

Figure 2

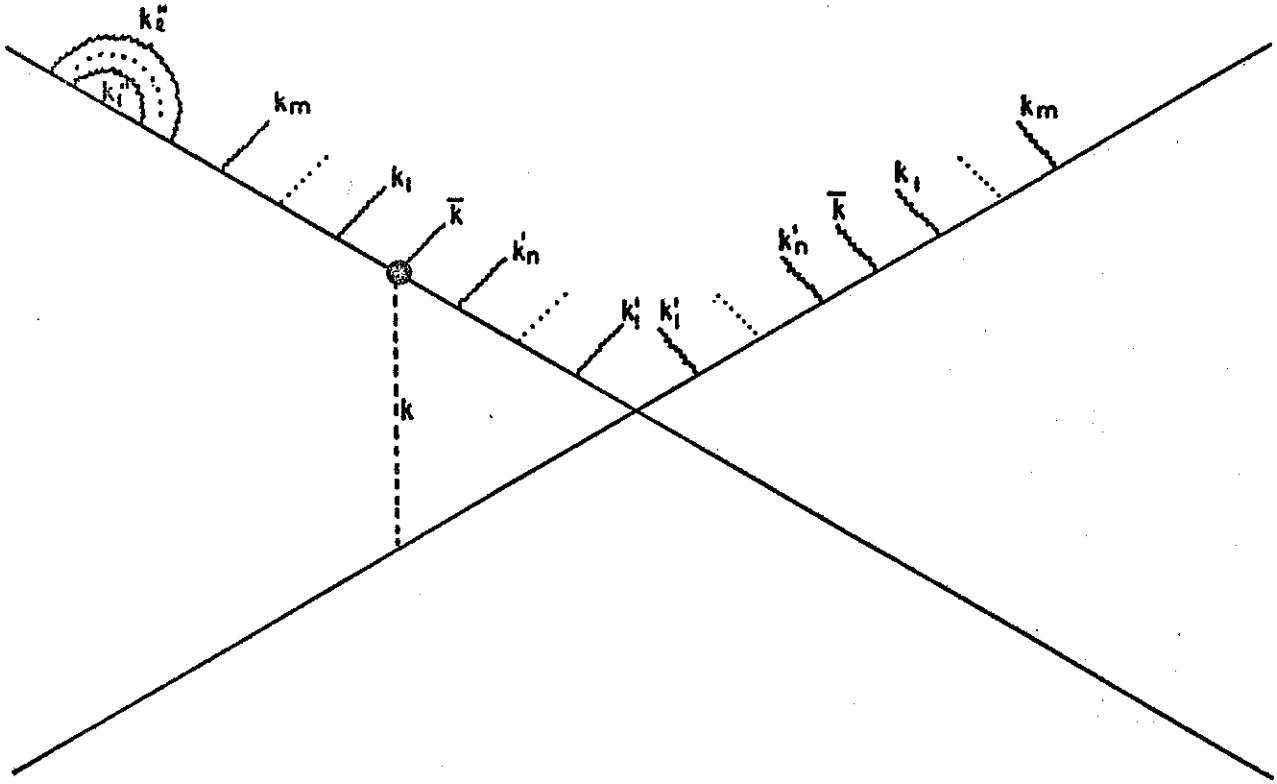

Figure 3

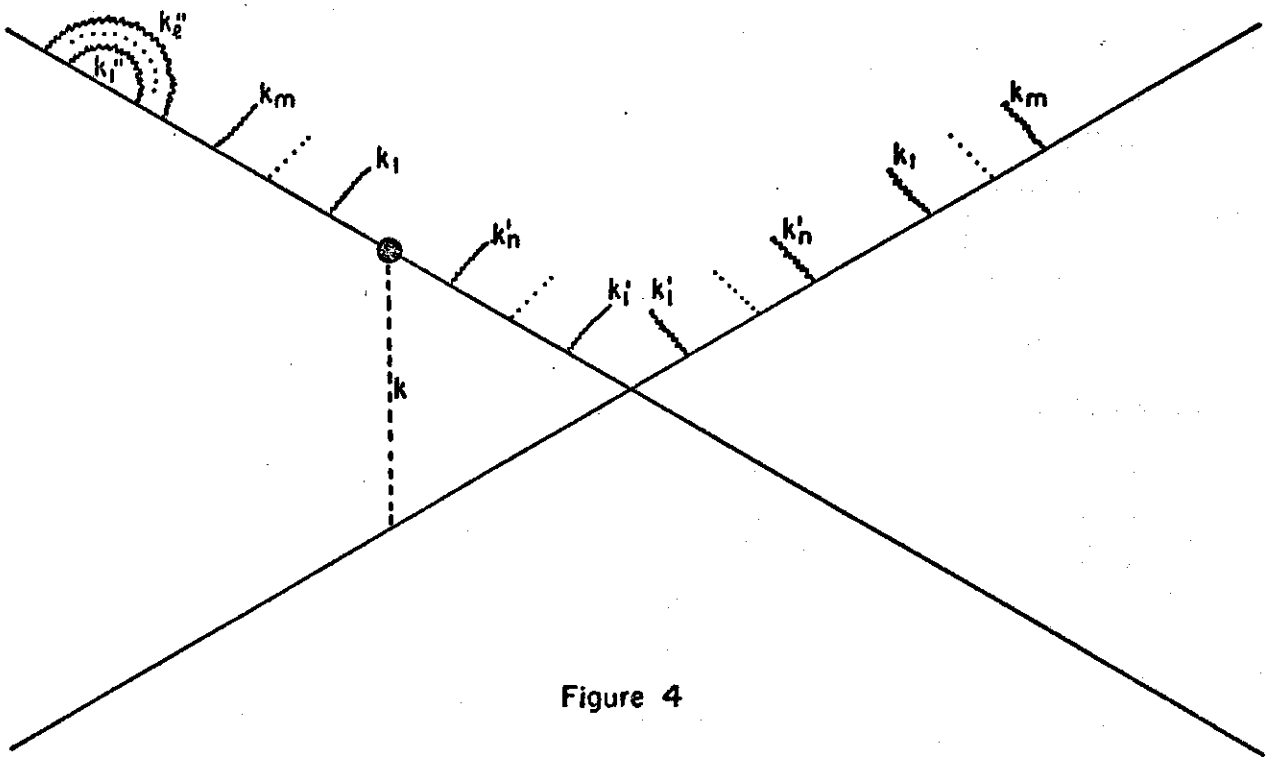

Figure 4

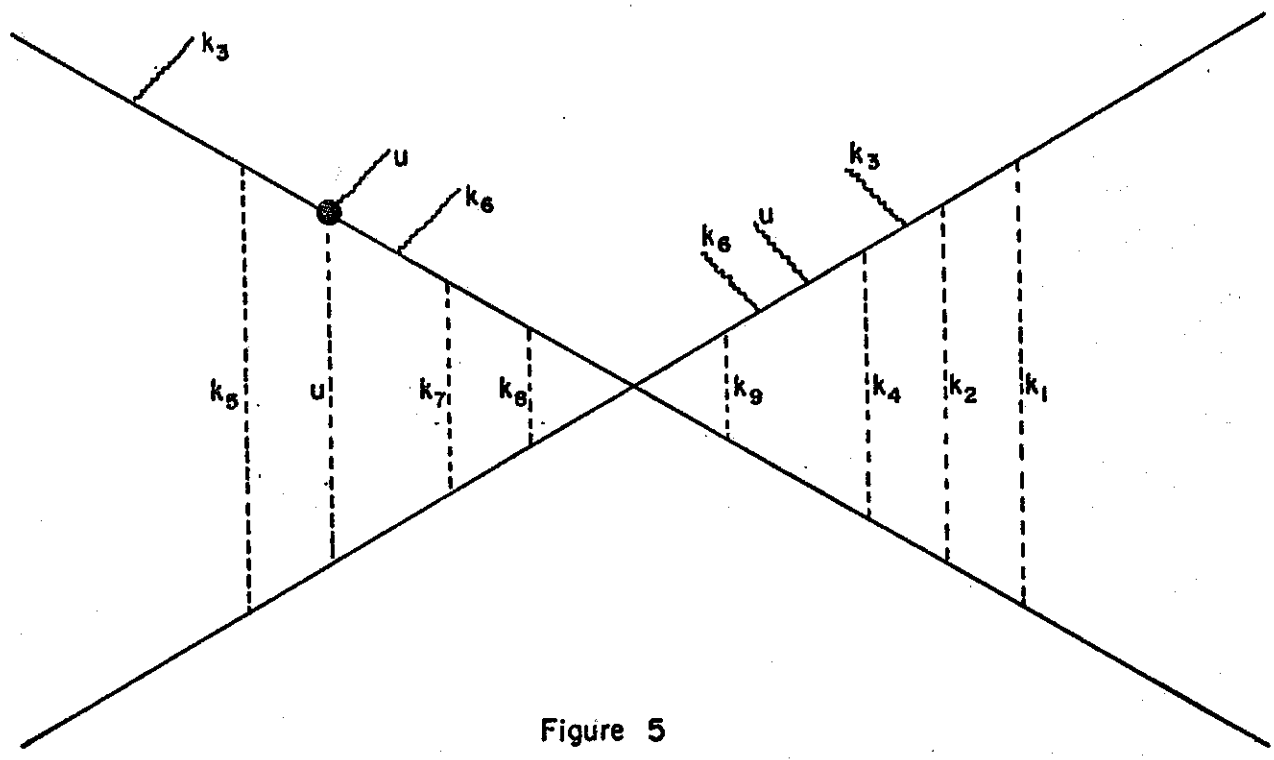

Figure 5

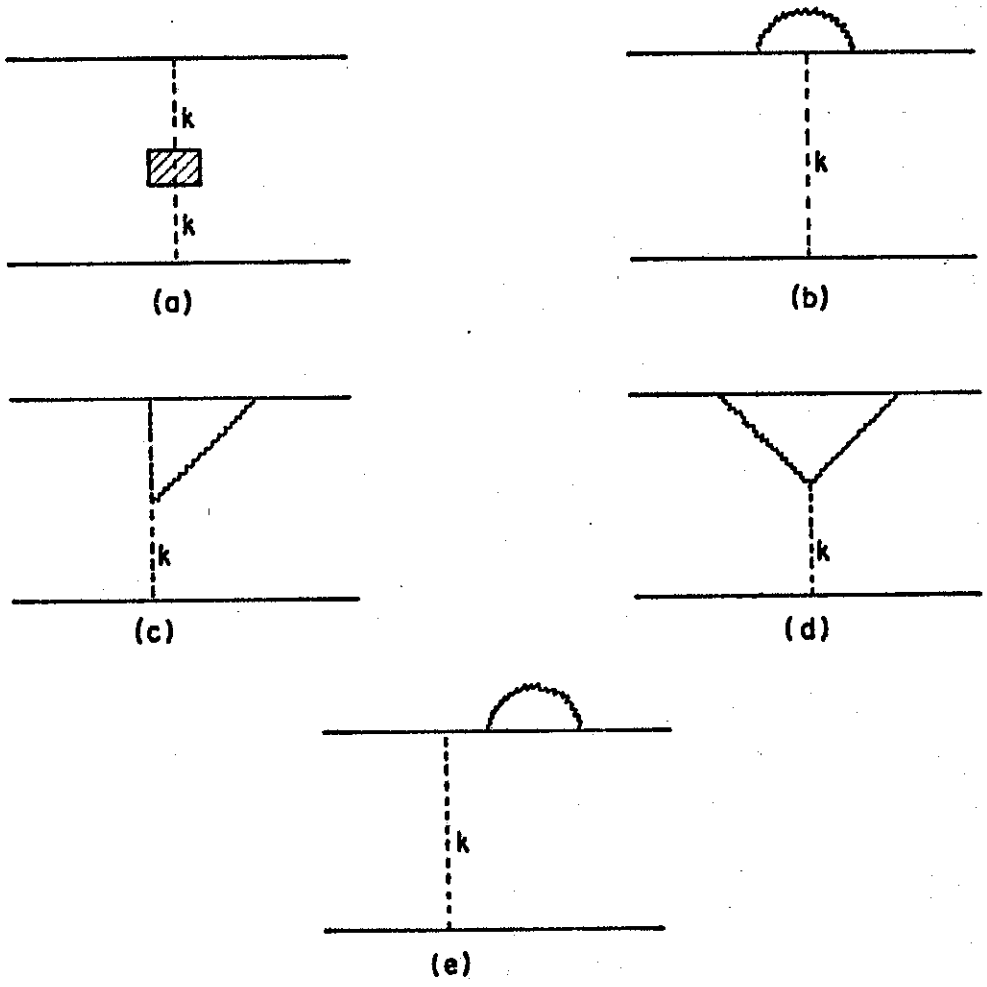

Figure 6

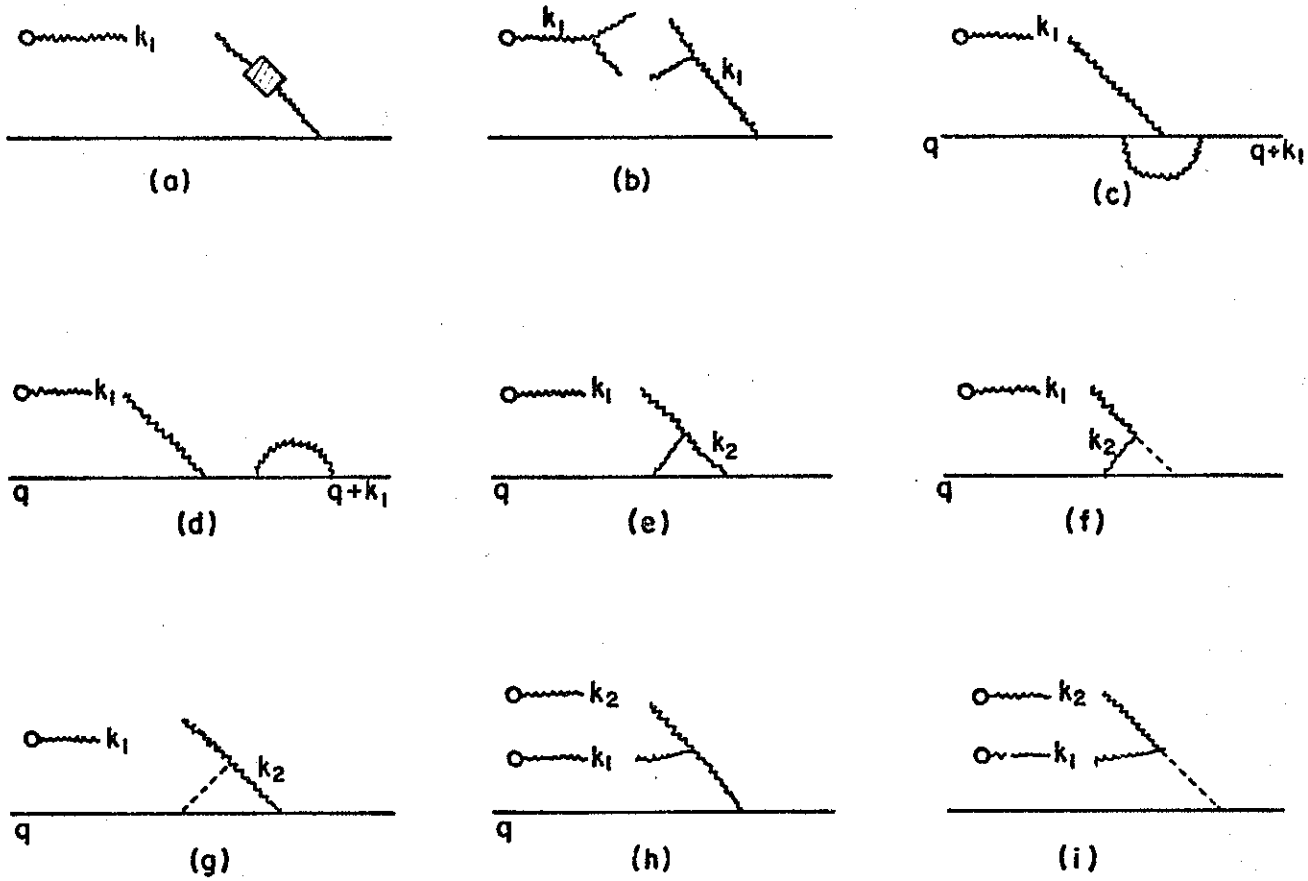

Figure 7

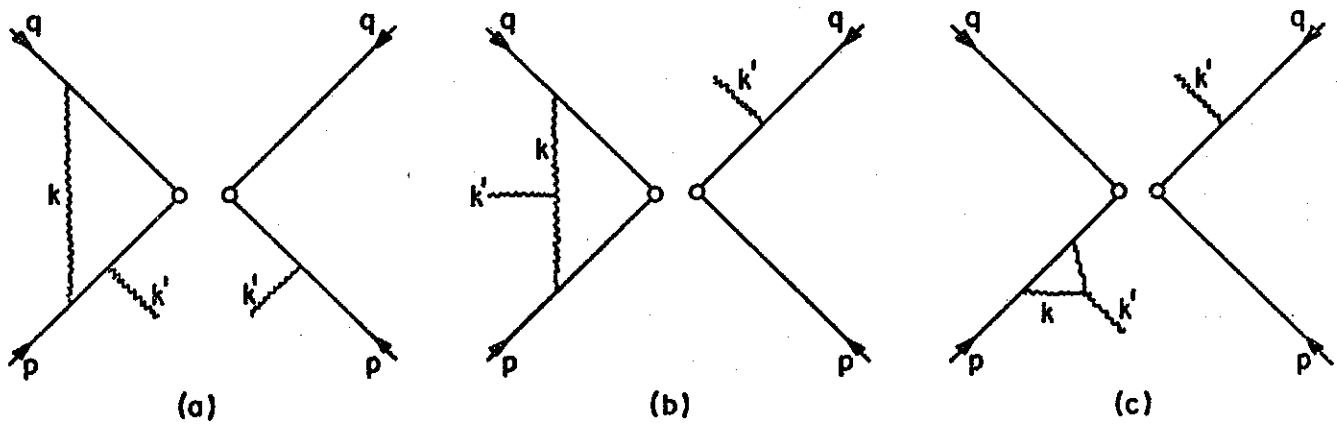

Figure 8

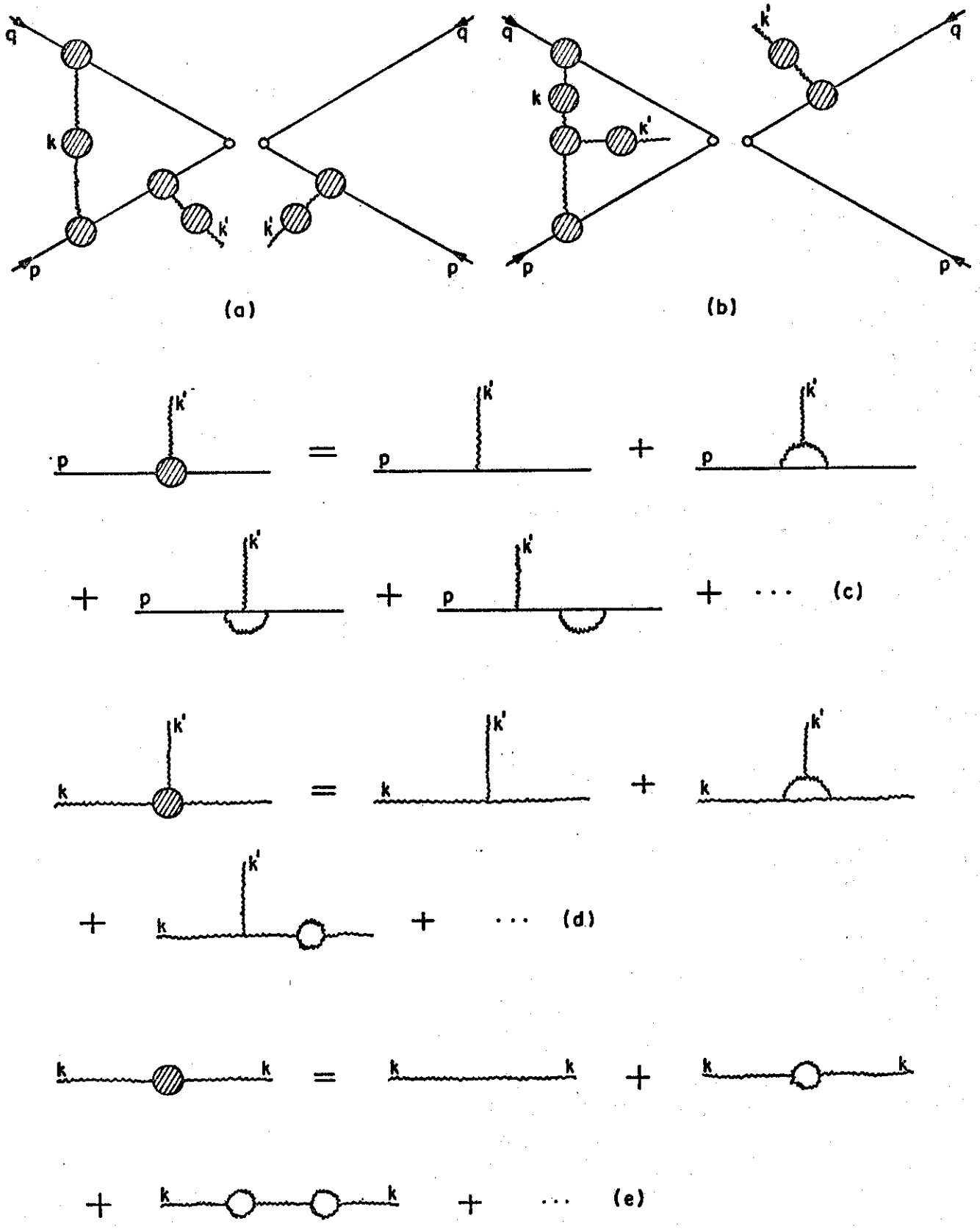

Figure 9